11th ANKARA INTERNATIONAL AEROSPACE CONFERENCE **AIAC-2021-034**
8-10 September 2021 - METU, Ankara TURKEY

A CODE TO DETERMINE THE STRUCTURE OF TURBULENCE USING QUANTIC BEHAVIOR OF TURBULENCE AND ITS APPLICATIONS

Elif Bekoğlu* , Ilgın Çolak† and Cahit Çıray‡
Middle East Technical University
Ankara, Turkey

ABSTRACT

One of the problems of turbulence is to know the properties of eddies such as sizes and energy contents. Spectral studies give the energy spectrum in terms of frequency. The task is to obtain information about the eddy sizes or wavelengths from the energy spectrum. The relation of wavenumber and frequency is associated with eddy sizes in turbulent flows. This relation is based on Taylor's frozen turbulence hypothesis and is frequently used in the literature. But this approach has some limitations and gives unrealistic results for large eddies. Therefore, the alternative methods or corrections to this approach are studied in the literature.

This study is based on an alternative approach called as Quantic Behavior of Turbulence. This approach explains the nature of turbulence with both wave and particle characteristics and presents a mathematical procedure to obtain a wavenumber corresponding to required frequency. The present study is started by generating a standard computer program. This program provides the energy spectrum from the spectral study and wavenumbers of each frequency by following the mathematical procedure of this approach. In the validation of this code, 10 test cases are used. After that, several different types of turbulent flows are analyzed by this program. As a result of these analyses, the wavenumbers for the entire frequency ranges are obtained. The energy spectrums are in line with the trends in the literature, and reasonable wavelengths are obtained for each frequency. This approach offers more realistic information about the eddies and hence contributes to the understanding of turbulent flow problems.

INTRODUCTION

Today, turbulent flow studies concentrate on learning the sizes, lifespans and energy contents of the eddies for solving the turbulent flow problems. This task is finding energy content related to an eddy via the energy spectrum. To able to do that, energy spectrum is used, which provides the energy content in the frequency range. Taylor's frozen turbulence hypothesis provides the scales of eddies by assuming a small time interval at which properties of eddies do not change significantly [Taylor, 1938]. In this hypothesis, the wavenumber and frequency relation is suggested using the

*GRA in Aerospace Engineering Department, Email: elif.bekoglu@metu.edu.tr
†GRA in Aerospace Engineering Department, Email: cilgin@metu.edu.tr
‡Ph.D; DIC; MS. Prof. (Em) of Fluid Mechanics in Aerospace Engineering Department, Email: cciray@metu.edu.tr

mean velocity,

$$k = \frac{\omega}{\overline{U}} \, , \tag{1}$$

where k is the wavenumber, ω is the angular frequency and $\overline{U}$ is mean velocity. This relation is defined as applicable to low turbulence intensity cases. Some studies in the literature show that Taylor's hypothesis causes a gross error observed in large-scale turbulent structures [del Alamo and Jimenez, 2009], [de Kat and Ganapathisubramani, 2015], [Yang and Howland, 2018], [Zaman and Hussain, 1981], and considering the limitations and accuracy of this method, a new approach is needed.

In the Quantic Behavior of Turbulence (QBT) suggested by C. Çıray [Ciray, 1980], the fluctuation velocity is assumed as the energy transport velocity, unlike Taylor's hypothesis. The suggested dispersion relation is

$$u = \frac{d\omega}{dk} \, . \tag{2}$$

In the present thesis study, a standard computer code based on QBT is generated, and using this code, several different turbulent flow structures are analyzed, and results are shown and discussed.

METHOD

The application of QBT includes two main steps. In the first step, spectral study is used, the energy spectrum is obtained from the instantaneous velocities measured by the experiment. In the second part, the mathematical procedure of QBT is followed, and the wavenumbers are calculated. The algorithm is shown in Fig. 1 and all these procedures are explained below.

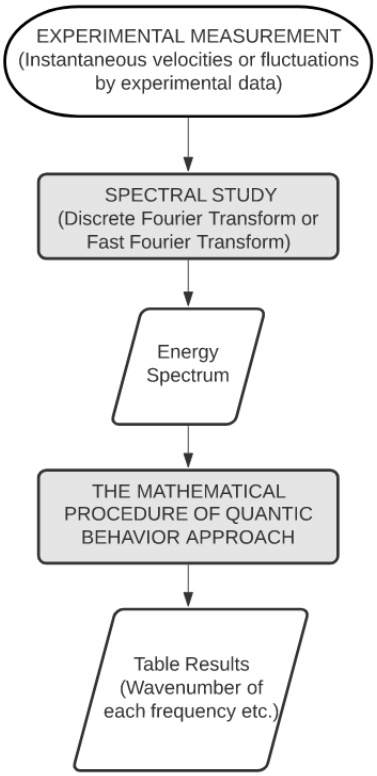

Figure 1: The flowchart of the algorithm

Spectral Study

In the spectral study, velocity fluctuations are represented as infinite sum of sines and cosines. This is the Fourier series representation [Ciray, 2013],

$$u(t) = 2\pi \int_0^\infty [a(n)cos(2\pi nt) + b(n)sin(2\pi nt)] \, dn \, , \tag{3}$$

where n is frequency, t is time and Fourier coefficients are represented as below,

$$a(n) = \frac{1}{\pi} \int_{-\infty}^{\infty} u(t)cos(2\pi nt) \, dt \, , \tag{4}$$

$$b(n) = \frac{1}{\pi} \int_{-\infty}^{\infty} u(t)sin(2\pi nt) \, dt \, . \tag{5}$$

Using Fourier integral, the kinetic energy contribution of each frequency interval can be obtained from the following velocity relation,

$$\overline{u}^2 = \pi^2 \int_0^\infty \frac{a(n)^2 + b(n)^2}{T} \, dn = \int_0^\infty E(n) \, dn \, , \tag{6}$$

where T is the period, and E is the spectrum function which is the energy density. In equation (6), "$E(n)dn$" means the kinetic energy contribution of frequency interval dn between n and $n + dn$

as shown in Fig. 2. This is the one-dimensional Taylor's spectrum and as can be seen from the same figure, the energy density is maximum in a frequency interval. But for very high and small frequencies, it is very small. Therefore, the outside of the n_1 and n_2 interval is not taken into account.

The Procedure of QBT

The usual relation of wavenumber and frequency is given in equation (1). But the following alternative relation (2) was introduced by C. Çıray with the detailed calculation steps [Ciray, 1980].

The relation (2) is based on the Quantic Behavior of Turbulence. QBT suggests that the turbulence has both wave and particle characteristics, and turbulence energy is carried by "**material packages of finite lifespan**" [Ciray, 2017]. Therefore, the fluctuation velocity is defined as the energy transport velocity (group velocity) of the package that exhibits wave-like behavior.

In the calculation of wavenumber, the characteristic information of the flow is required, and this information is obtained by the characteristics of the spectrum in this equation,

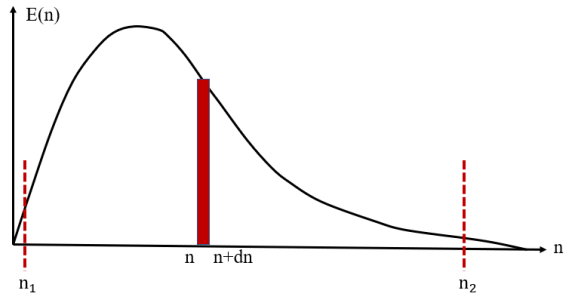

Figure 2: 1-D Taylor's spectrum

$$\int_{-\infty}^{\infty} P(y)u^2\,dy = u'^2 \int_0^{\infty} G(f)\,df\ , \tag{7}$$

where $P(y)$ is Probability Density Function (PDF), and a Maxwell type distribution is modified by C. Çıray and it becomes,

$$P(y) = P(1)y^m exp\left[A^m(1-y^m)\right]\ , \tag{8}$$

in this approach. In equation (8), $P(1)$, A and m are constants depending on turbulence intensity. In equation (7), u' is the root-mean-square (rms) of the velocity fluctuation, $u(f)$, and $y(f)$ is the non-dimensional instantaneous velocity. In addition, G is the spectrum function, $G(f) = E(f)/u'^2$, which is the energy density divided by u'^2 and f is frequency.

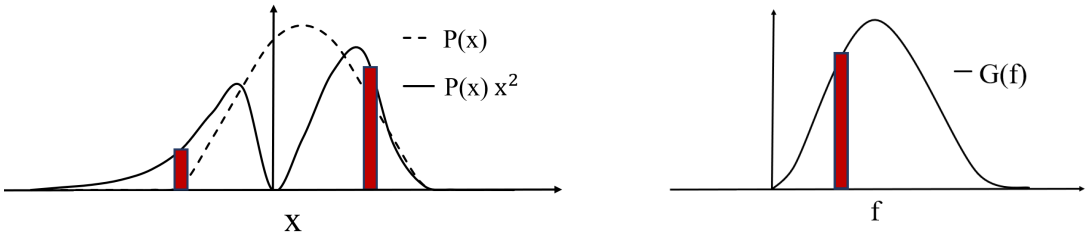

Figure 3: The relation between Probability Density Function and Spectrum Function (non-dimensional fluctuation velocity x, $x(f) = u(f)/u'$ and its relation with the non-dimensional instantaneous velocity, y, is $y = 1 + Ix$ where I is turbulence intensity.)

Fig. 3 is a representation of equation (7). As can be seen from Fig. 3, the chosen PDF is skewed. It means that the probabilities around $+u$ and $-u$ are different. But both velocities contribute together to kinetic energy at the same frequency, and this information is provided from the spectral study. This can be seen in the right-hand-side of Fig. 3 and equation (7). Therefore, equation (7) can be solved for $u(f)$ with the knowledge of spectrum information of experimental data. Then, the wavenumber of each frequency can be calculated by using equation (2).

RESULTS AND DISCUSSION

In this section, some results of the applications of QBT are presented. The first results are obtained from the instantaneous velocity data of Dogan et al.-Case A, which is a boundary layer data. By QBT, this case is analyzed, and the length scales are compared with those presented in Dogan et al. [Dogan, Hanson and Ganapathisubramani, 2016].

Results of Dogan et al.-Case A by QBT

The given method is applied to one of the boundary layer data cases of Dogan et al. [Dogan, Hanson and Ganapathisubramani, 2016]. These experiments are carried out in a suction-type wind tunnel. The cross-section of this wind tunnel is 0.9 m x 0.6 m, and its length is 4.5 m. For case A, the turbulence is generated by using the cut-out wings as an active grid, and the length of the square mesh of the active grid (M) is 81 mm. For these experiments, a 4.2 m long flat plate is placed at 0.135 m height of the bottom of the test section, and the boundary layer is created over the flat plate as shown in Fig. 4. The instantaneous velocities are measured at 28 different y-locations within the boundary layer and at a fixed location in freestream at location $x = 43M$ for 6 minutes with a sampling rate of 20 kHz.

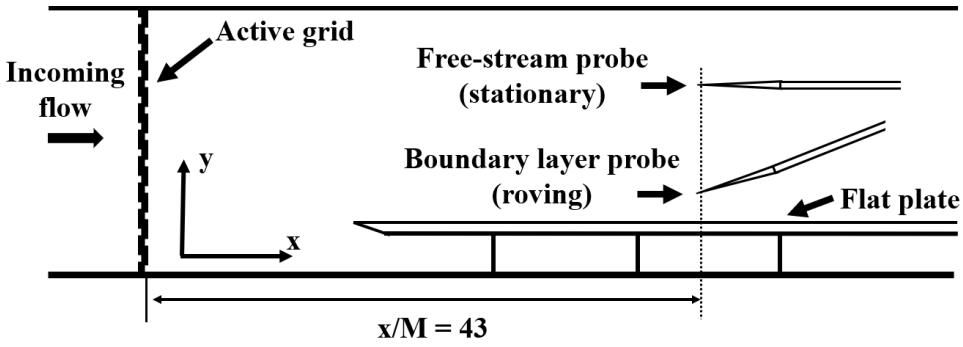

Figure 4: Schematic of test section of boundary layer experiment of Dogan et al. [Dogan, Hanson and Ganapathisubramani, 2016] reproduced from their Figure 1

The velocity profile at $x = 43M$ is shown in Fig. 5. In this study, only points 1, 2, 3 and 4 (free-stream) are selected to understand the change in both inside the boundary layer and out in the free-stream. They are given in the same figure for a clear comparison.

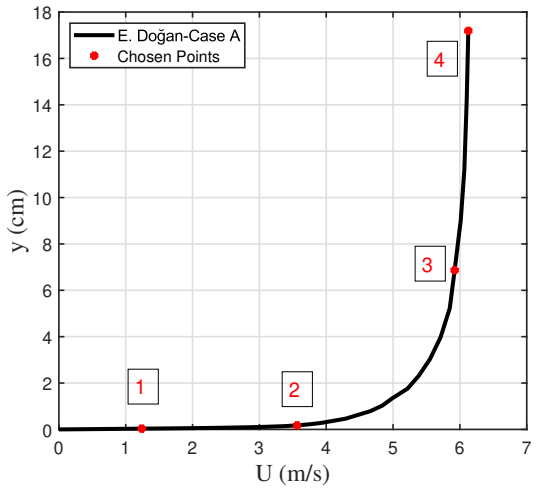

Figure 5: Boundary layer profile of Dogan et al.-Case A and the four points chosen for analysis in this study

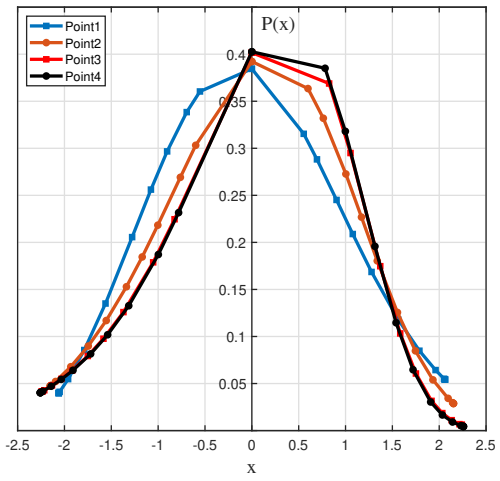

Figure 6: The PDFs of the chosen points Dogan et al.-Case A

As shown in Fig. 6, the PDFs of these points are plotted as a function of non-dimensional fluctuation velocity, $x(f) = u(f)/u'$. With the knowledge of the mean velocity and the rms of the instantaneous fluctuations, the PDF is obtained for each measurement uniquely. By following the mathematical procedure of QBT, these PDFs provide wavenumbers and other significant results to be explained in the paper. Fig. 7 shows the energy spectrums for all wavenumbers obtained from these four points and, it should be pointed out that these are valid for all frequency ranges especially including large eddies.

As an expected result, large eddies correspond to the smaller wavenumbers, and they have different characteristics depending on boundary conditions. In Fig. 7, the slope of the energy spectrum, -5/3, in the inertial subrange is consistent with the previous studies on energy spectrum in the literature, and this range is observed between 50 Hz - 500 Hz. The frequency of approximately 200 Hz is shown in the figure as representative for this range. For the frequencies higher than 1000 Hz, energy dissipates very quickly which is consistent with the results obtained in the literature about the dissipating eddies. Another observation is that the energy spectrum curves approaches the freestream curve as the measurement point approaches the freestream.

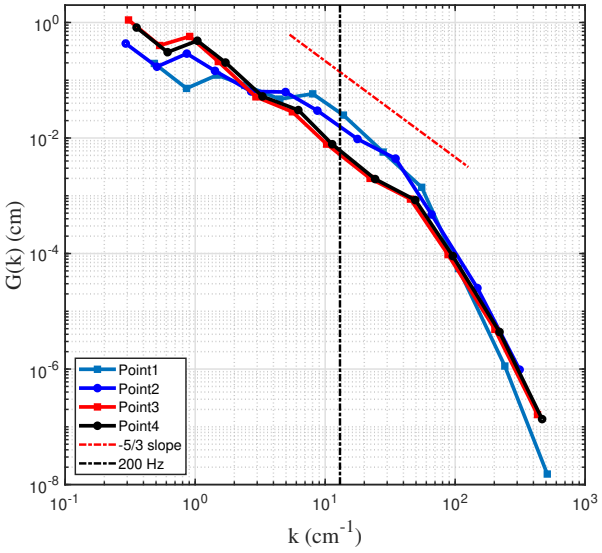

Figure 7: The energy spectrum of the chosen points of Dogan et al.-Case A

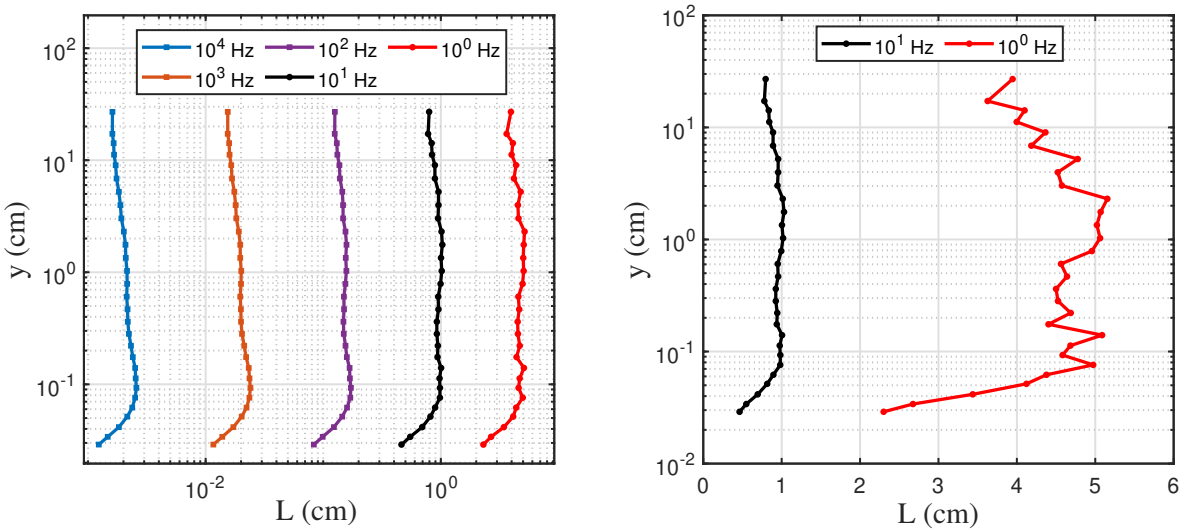

Figure 8: The size variation of eddies at different frequencies along the boundary layer; in logarithmic scale of all sizes (a), in normal scale of larger sizes (b).

The size and the lifespans of eddies also give some striking results. As can be seen from Fig. 8 and 9, sizes and lifespans of the large eddies at small frequencies are the highest, and their behavior changes irregularly. However, all frequency curves appear similar on the plot with a logarithmic

scale; the change in eddy size and lifespan increases as the frequencies decrease, as shown clearly in normal scale plots. When the frequency increases, the sizes and lifespans of eddies decreases, and the curve behavior loses its uniqueness and takes on a universal shape. But still, for each curve, the most evident change appears near the wall, and larger size and lifespan are found at high rms values.

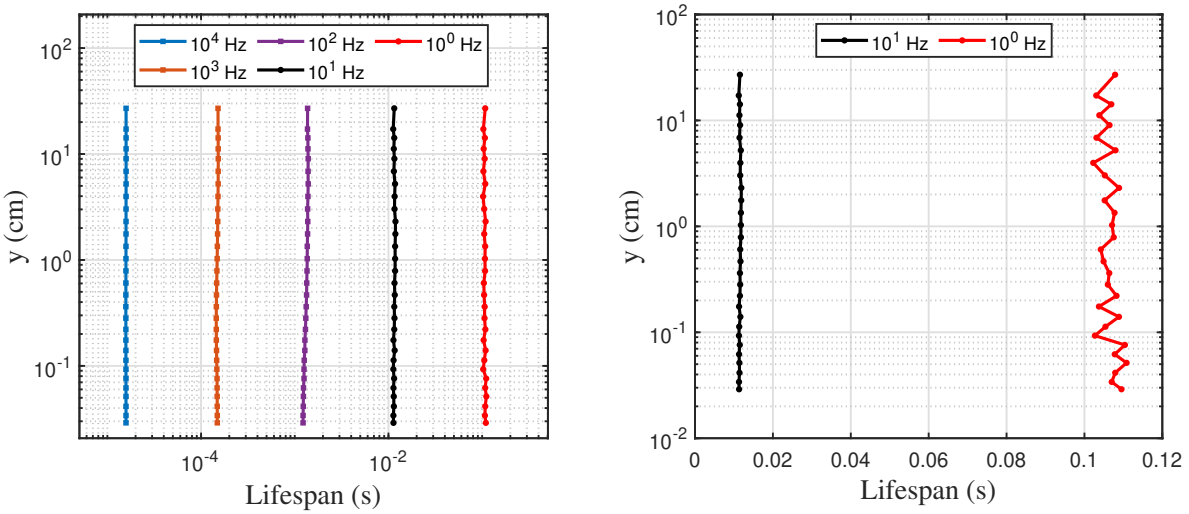

(a) (b)

Figure 9: The lifespan variation of eddies at different frequencies along the boundary layer; in logarithmic scale of all lifespans (a), in normal scale of larger lifespans (b).

In Table 1, the size and lifespan of the largest eddies at 1 Hz and smallest eddies at 10^4 Hz are given. Although the size of the smallest eddies is on the order of one-tenth of a millimeter, the size of the largest eddies is found in centimeters, which is a comparable value with the boundary layer thickness (11 cm). Also, these sizes do not exceed the physical boundaries of the flow. The order of the lifespan of these largest eddies is one-tenth of a second, while those of the smallest eddies are in the microsecond level.

Measurement Point -	Size of the Largest Eddy (at 1 Hz)	Size of the Smallest Eddy (at 10^4 Hz)	Lifespan of the Largest Eddy (at 1 Hz)	Lifespan of the Smallest Eddy (at 10^4 Hz)
POINT 1	2.675 cm	0.147 mm	0.107 s	15.81 μs
POINT 2	4.403 cm	0.240 mm	0.104 s	15.76 μs
POINT 3	4.184 cm	0.175 mm	0.103 s	15.84 μs
POINT 4	3.627 cm	0.161 mm	0.103 s	15.83 μs

Table 1: The size and lifespan of the largest and smallest eddies of chosen points

The results of Point 1 and Point 4 (free-stream) are given in Table 2 and 3, respectively. The mean velocity $\overline{U}$, rms of velocity fluctuations u', and turbulence intensity I are shown above the table. Other shown parameters are ΔG, which is the kinetic energy contribution of each frequency f interval, nondimensional instantaneous velocity x, wavenumber k, wavelength L. Also, P_R and P_L are the right and left side values of PDF at given x locations, respectively.

$\overline{U}$ =1.240 m/s I=0.3639 u'=45.13 cm/s

f	ΔG	x	k	L	$P_R(x)$	$P_L(x)$
Hz	-	-	cm^{-1}	cm	-	-
0		-	-	-	0.3845	0.3845
	0.0436					
1		0.5536	0.3738	2.675	0.3154	0.3604
	0.0377					
2		0.6951	0.5958	1.676	0.2882	0.3385
	0.0863					
5		0.9041	1.119	0.8936	0.2451	0.2967
	0.0966					
10		1.077	1.822	0.5489	0.2089	0.2561
	0.1389					
20		1.278	3.004	0.3329	0.1686	0.2056
	0.2417					
50		1.562	5.946	0.1682	0.1180	0.1350
	0.1850					
100		1.788	10.101	0.0990	0.0849	0.0856
	0.1189					
200		1.961	17.527	0.0571	0.0643	0.0547
	0.0475					
500		2.051	38.345	0.0261	0.0551	0.0412
	0.0037					
1000		2.061	72.203	0.0138	0.0542	0.0400
	0.0002					
2000		2.061	139.76	0.0072	0.0542	0.0399
	0.000005					
5000		2.061	342.40	0.0029	0.0542	0.0399
	0.000001					
10000		2.061	680.14	0.0015	0.0542	0.0399

Table 2: Table Results of Dogan et al.-Case A-Point 1

As can be seen from Table 2 and 3, the kinetic energy contribution of the eddies is decreasing with increasing frequencies. The kinetic energy contribution of eddies at a frequency higher than 200 Hz is almost 5% and 3% of all kinetic energy for Point 1 and 4 (free-stream), respectively.

Table 2 and 3 also show that the rise of the non-dimensional fluctuation velocity reduces with the decrease of eddy sizes and PDF values and becomes fixed at a frequency such as 1000 Hz for Point 1 and 2000 Hz for Point 4. In other words, the probabilities of the existence of these fluctuations become smaller with higher frequencies. This is valid for both negative and positive fluctuations. Even though, the positive and negative fluctuation velocities have different probabilities due to the skewness of PDFs; they behave similarly. Finally, the wavelengths (sizes) and wavenumbers of eddies at corresponding frequencies are obtained and shown in Table 2 and 3.

$\overline{U}$ =6.126 m/s I=0.0735 u'=45.03 cm/s

f	ΔG	x	k	L	$P_R(x)$	$P_L(x)$
Hz	-	-	cm^{-1}	cm	-	-
0		-	-	-	0.4026	0.4026
	0.1282					
1		0.7817	0.2757	3.627	0.3851	0.2316
	0.1109					
2		0.9981	0.4325	2.312	0.3181	0.1871
	0.2365					
5		1.314	0.7946	1.259	0.1958	0.1327
	0.1735					
10		1.539	1.284	0.7790	0.1146	0.1018
	0.1211					
20		1.721	2.140	0.4673	0.0647	0.815
	0.1077					
50		1.909	4.447	0.2249	0.0304	0.0641
	0.0522					
100		2.034	7.986	0.1252	0.0166	0.0544
	0.0373					
200		2.142	14.67	0.0682	0.0091	0.0471
	0.0262					
500		2.232	33.81	0.0296	0.0052	0.0418
	0.0056					
1000		2.255	64.91	0.0154	0.0045	0.0405
	0.0008					
2000		2.258	126.75	0.0079	0.0044	0.0403
	0.00004					
5000		2.258	312.11	0.0032	0.0044	0.0403
	0.000007					
10000		2.258	621.03	0.0016	0.0044	0.0403

Table 3: Table Results of Dogan et al.-Case A-Point 4 (free-stream)

Comparison of Length Scales of Dogan et al.-Case A

In this section, the obtained length scales by QBT are compared with those of the study of Dogan et al. [Dogan, Hanson and Ganapathisubramani, 2016]. First, the scales determined for free-stream will be compared. After that, the comparisons will be made for the scales within the boundary layer.

Comparison of Length Scales of Dogan et al.-Case A in the Free-stream:

In Table 4, the calculated length scales for free-stream in Dogan et al.'s study and by QBT are shown.

Parameters		**Dogan et al.'s Results**	**QBT Results**
Integral scale 1	L_0 (cm)	17.0	3.63
Integral scale 2	L_0^* (cm)	45.3	3.63
Taylor microscale	λ_0 (cm)	1.08	0.80
Kolmogorov scale	η_0 (cm)	0.030	0.002
The most energetic scale	L_{en} (cm)	162	1.31

Table 4: Comparison of the length scales of free-stream

In Dogan et al.'s study, the integral scale 1, given as 17 cm, is calculated from the first zero cross of the integrated normalized auto-correlation, while the relation which defines the integral scale with rms of the fluctuations and the turbulence energy dissipation rate calculated based on Taylor's hypothesis, by Mydlarski & Warhaft [Mydlarski and Warhaft, 1996], is used for the calculation of integral scale 2 as 45 cm. But in Dogan et al.'s study, the most energetic scales are given as the main focus. Therefore, the corresponding wavelength to the spectral peak of pre-multiplied energy spectra is considered as the most energetic length scale. The Taylor microscale and Kolmogorov scale are found from their standard definitions, and these definitions include the turbulence energy dissipation rate calculated by using Taylor's hypothesis.

The size of the largest eddies in the freestream found by QBT is compared with the mentioned integral scales, and the difference is apparent. But the most obvious difference is observed for the most energetic eddies. The size of the most energetic eddies is found as 162 cm in Dogan et al.'s results, while it is found as 1.31 cm by QBT. This size, 162 cm, is significantly larger than the integral scales and comparable with the length of the flat plate and tunnel. But the value of 1.31 cm is less than the size of the largest eddies by QBT, 3.63 cm. Therefore, this approach gives more justifiable results with the understanding of the energy spectrum.

The Taylor microscale is related to the eddies that begin to be affected by viscous dissipation. To compare results with the Taylor microscale, the scale is taken as the size at the beginning of the inertial subrange (-5/3 slope). Both results are found similar. Finally, the size of the smallest eddies is compared with the Kolmogorov scale. This scale by QBT is found as 0.002 cm and approximately one-tenth of Dogan et al.'s result.

Comparison of Length Scales of Dogan et al.-Case A within the Boundary Layer:

The obtained length scales for the boundary layer by two studies are shown in Table 5.

Parameters		**Dogan et al.'s Results**	**QBT Results**
Boundary layer thickness	δ (cm)	11.0	-
Turbulence length scale	L_e (cm)	51.2	5.15
The most energetic scale	L_{en} (cm)	113	0.541

Table 5: Comparison of the length scales of boundary layer

L_e is a turbulence length scale, and its definition comes from the decay power law of the grid turbulence [Castro, 1984]. But in Dogan et al.'s study, instead of L_e, the most energetic scale is chosen as the focus of the study. In that study, the corresponding wavelength of the spectral peak of the pre-multiplied energy spectra is taken as the most energetic length scale and is found as 113 cm. On the other hand, in the present study, the largest size observed within the boundary layer comes out as 5.15 cm which is one-tenth of the turbulence length scale L_e. But the most apparent difference is found between the most energetic scales L_{en}. Dogan et al.'s most energetic scale is approximately two hundred times of the scale obtained by QBT.

The sizes of eddies at frequencies of 5 Hz, 10 Hz, 20 Hz, and 50 Hz by QBT are shown in Fig. 10. In the same figure, Taylor microscales which express the eddies that start to be affected by viscous dissipation, are also plotted. It is observed that Taylor microscales are close to the sizes of eddies at 50 Hz near the wall. When the distance increases from the wall, the Taylor microscales approach to the size of the large eddies. Therefore, the Taylor microscales depart from its definition with increasing distance from the wall.

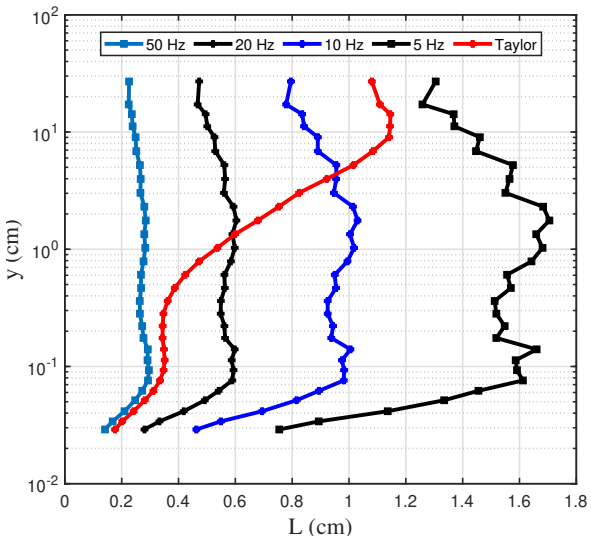

Figure 10: The comparison of the Taylor microscales with the sizes of eddies at different frequencies found by QBT along the boundary layer

The energy distribution in the boundary layer obtained by QBT, is given in Fig. 11 where $G(k)$ is the normalized spectrum function as mentioned before in equation (7). This contour plot in Fig. 11 is very similar to Dogan et al.'s results obtained by comparing the energy distribution and local spectral peaks. The locations of these peaks are found the same, but the corresponding normalized wavelengths are very different. It should also be noted that the wavelengths or sizes obtained by QBT are found to be smaller than the sizes used in the literature. This is especially true for the large eddies.

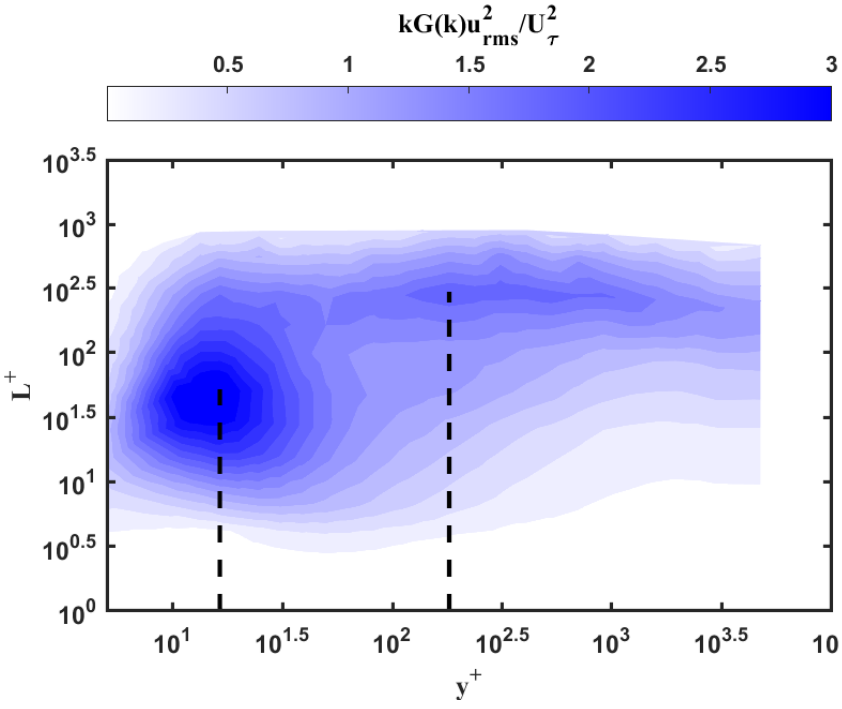

Figure 11: The energy distribution along the boundary layer; the non-dimensional wall distance $y^+ = \frac{yU_\tau}{\nu}$ in x-axis, the normalized wavelength $L^+ = \frac{LU_\tau}{\nu}$ in y-axis where skin friction velocity, $U_\tau = 0.27m/s$ and kinematic viscosity of air, $\nu = 1.6 * 10^{-5}m^2/s$, taken from the experiments of Dogan et al. (Dashed lines show the local spectral peaks.)

Another observation is that the energies shown in Fig. 11 are higher than those of Dogan et al.'s results. This is an expected result because energy is calculated by multiplying wavenumber (or dividing wavelength) and by QBT the higher wavenumbers (or smaller wavelengths) are obtained.

Results of MVG data analysis by QBT

Micro Vortex Generator is a simple device, generally has a geometry of a ramp or a vane, that creates miniature vortices and mixes the upper and lower portions within the boundary layer. As a result, energy is transferred from the upper portions to the lower portions and the kinetic energy of the lower portions are increased. It is one of the methods for delaying the separation by creating more energetic boundary layers. [Sun, 2015]

Micro Vortex Generator Data is obtained from the experiment conducted by Akpolat for his PhD research in progress with his kind permission. The experiment is carried out at METU Center for Wind Energy (RÜZGEM). The data is analyzed by the given method of QBT. In the experiment, a Micro Vortex Generator (MVG) is located 6.2 m from the inlet of the tunnel. HWA measurements were carried out at 324 mm downstream of the MVG, corresponding to z/h=10.8. The boundary layer probe employed for the measurements was placed 10 mm away from the bottom wall of the wind tunnel. The probe was traversed vertically up to 162 mm with increments of 2 mm for each measurement. The sampling time was chosen to be 30 s with a sampling frequency of 10 kHz. For the experiment METUWIND/RUZGEM C3 Medium Scale Suction Type Wind Tunnel is used and free-stream velocity was approximately 10 m/s.

There are no measurements for 12 mm and 112 mm positions. Thus, the data is obtained for 74 different points. For the analysis 7 different data points are chosen : 14 mm, 18 mm, 22 mm, 26 mm, 34 mm, 54 mm and 74 mm. The same measurement procedure is repeated in the same wind tunnel without a MVG for the same traverse points on the 6.2 m distance from the inlet, as in the first case. Thus, undisturbed boundary layer data is also obtained. For the analysis, boundary layer velocity profiles are plotted for each case. Then, using aforementioned method of QBT, PDFs of data points for MVG case are obtained. Also, energy spectrum based on frequency and wavenumber are obtained for each data point and for each case. Results of this analysis are presented in the following pages.

h[mm]	w[mm]	c[mm]	α[°]
30	184	212	8.3

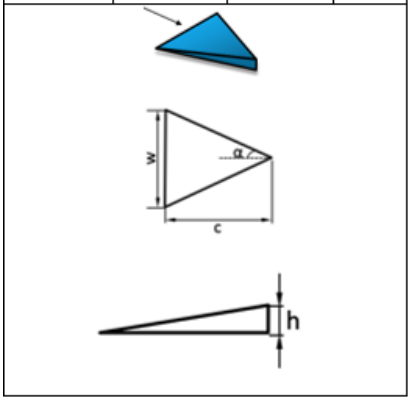

Figure 12: Dimensions of MVG [Akpolat et al., 2021]

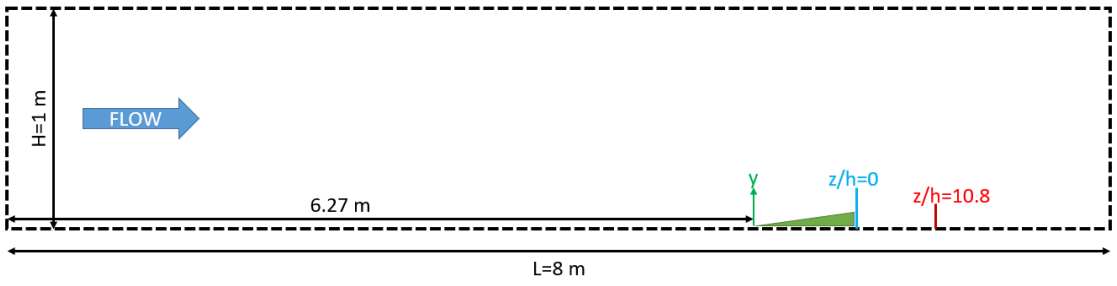

Figure 13: Schematic for the placement of MVG inside the tunnel [Akpolat et al., 2021]

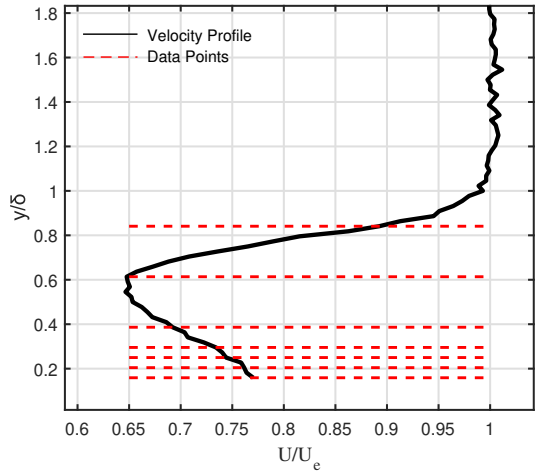

Figure 14: Boundary layer velocity profile for MVG case

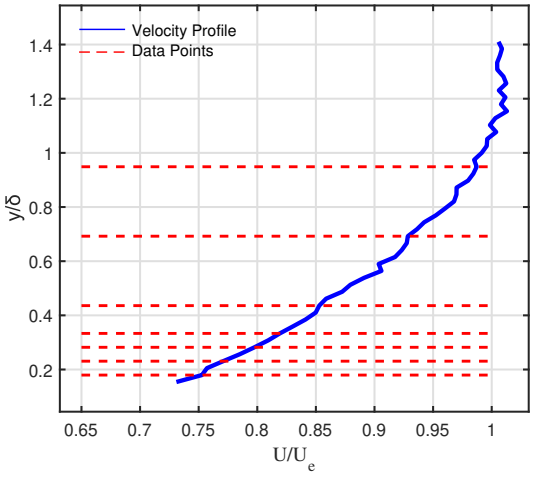

Figure 15: Velocity profile of the undisturbed boundary layer

As can be seen from the Fig. 14 a wake behind the MVG can be observed in the lower regions of the boundary layer. Boundary layer thickness for the undisturbed case is calculated as 78 mm whereas for the MVG case it is 88 mm. Thus, there is a 88% increase in the boundary layer thickness in the MVG case compared to the undisturbed case.

PDFs for three different traverse points are plotted by applying the aforementioned procedures of QBT method. Positions of these points within the boundary layer can be seen from the Fig. 14.

From the Fig. 17 and Fig. 18, energy spectrum based on frequency and wavenumber can be observed, respectively. Spectrum is plotted at each point and for each case. Same colors represent the same data points and dashed lines represent the MVG case where full lines represent undisturbed case.

As expected the energy densities for the case with MVG are higher than the ones for the undisturbed case, especially near the tunnel wall where the large eddies are formed. This shows that MVG application is successful. This is the situation for all points except 74 mm where no significant difference between MVG case and undisturbed case is observed. Considering that 74 mm is 84% of the boundary layer thickness for MVG case, it can be concluded that MVG loses it effectiveness for the upper regions of the boundary layer.

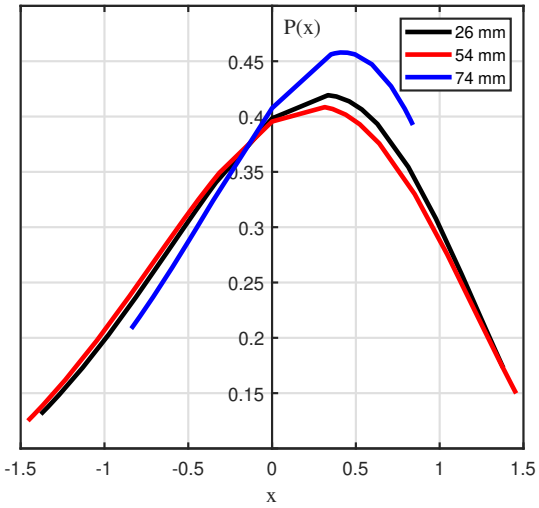

Figure 16: PDFs of three different traverse points: 26 mm, 54 mm and 74 mm

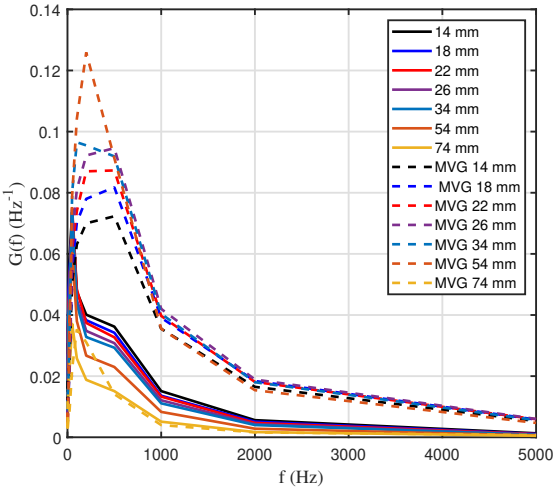

Figure 17: Spectrum based on frequency for each data point

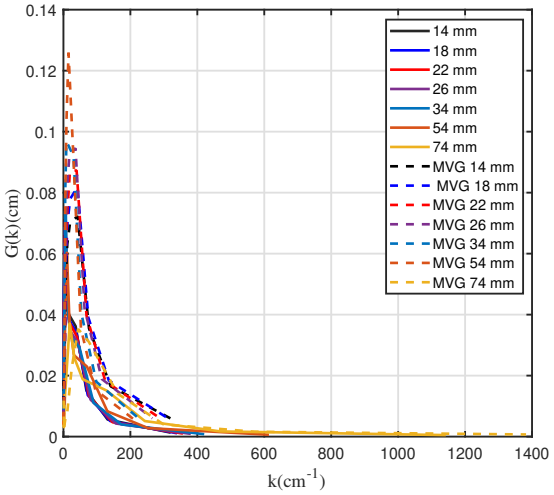

Figure 18: Spectrum based on wavenumber for each data point

It can be observed that as frequency increases energy densities are decreasing, which is a result of energy dissipation between eddies. When the distance from the bottom wall is increased, a constant decrease in energy densities can be clearly observed for 200-1500 Hz interval for undisturbed case. However, in the same frequency range, for the case with MVG, behaviour of energy densities is not quite straightforward. Especially in the low frequency range, it is obvious that the energy densities are increasing with increasing traverse position. Then, for the frequencies between 500 Hz and 1500 Hz, no direct relation between the traverse position and energy densities can be inferred. This situation can be explained by the fact that MVG mixes the upper and lower portions of the flow within the boundary layer.

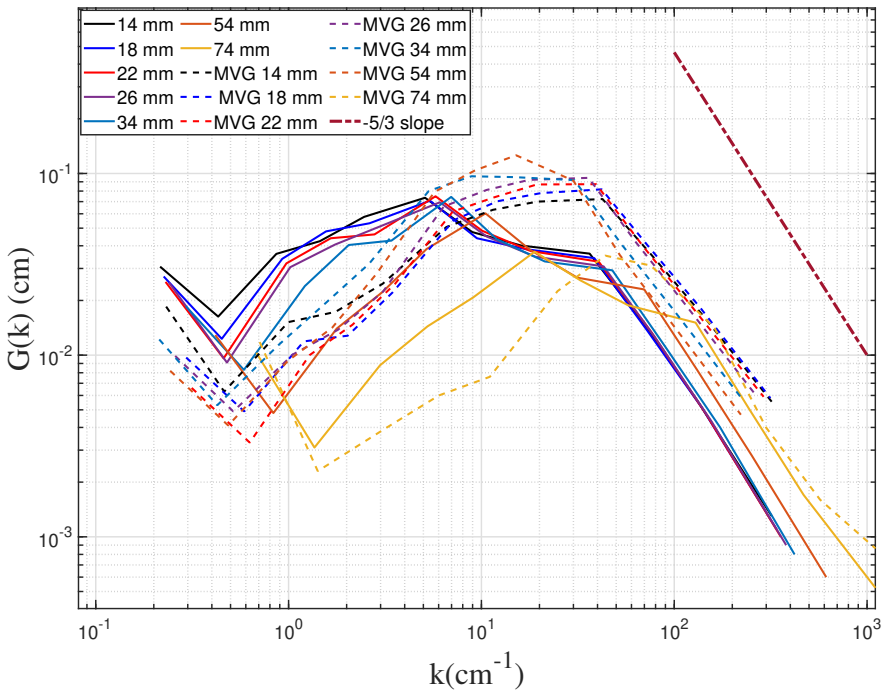

Figure 19: Spectrum based on wavenumber in logarithmic scale

For the spectrum based on wavenumber, smaller wavenumbers correspond to larger eddie sizes. The slope of the energy spectrum in the inertial subrange is about -5/3 which is consistent with the studies in the literature. Frequency interval for this subrange is 500-5000 Hz and 1000 Hz can be taken as representative value.

Traverse Position(mm)	Largest Wavelength(cm)		Turbulence Intensity(-)		Mean Velocity(m/s)	
-	Undisturbed	MVG	Undisturbed	MVG	Undisturbed	MVG
14	4.6361	4.3137	0.0991	0.0975	7.7533	7.7533
18	4.4425	3.3962	0.0934	0.1028	7.9402	7.9402
22	4.3440	3.1800	0.0874	0.1117	8.2151	8.2151
26	4.1736	3.8723	0.0814	0.1203	8.4383	8.4383
34	3.4106	4.6859	0.0731	0.1404	8.7846	8.7846
54	2.3992	4.1116	0.0516	0.1541	9.5629	9.5629
74	1.4689	1.4117	0.0311	0.0269	10.1677	10.1677

Table 6: Comparison of undisturbed and MVG cases based on largest wavelength, turbulence intensity and mean velocity

The largest wavelength is 4.6361 cm and 4.3137 cm for the undisturbed case and MVG case, respectively. This is a significant result since the wavelength represent the eddy size and the largest eddy size must be reasonable when the physical boundaries of the experiment are considered. The boundary layer thickness can be taken as the dimension for the physical domain for these experiments and they are 88 mm and 78 mm for the MVG case and undisturbed case, respectively. Thus, the largest eddies are smaller than the physical boundaries of the experiment for each case. This shows that QBT can predict physically meaningful eddy sizes.
The effect of MVG can be observed from the largest wavelengths listed for each case. As expected, there are larger eddies near the boundaries, i.e. the bottom wall of the tunnel for undisturbed case. Parallel to that, there is a continuous decrease in wavelength with increasing traverse position for undisturbed case. However, for the MVG case first there is a decrease in wavelength up to 22 mm traverse position, then wavelength increases up to 54 mm position. It means that larger eddies are produced in respectively upper regions when MVG is employed. This phenomenon can be explained by the fact that MVG is a device that mixes upper and lower layers of the flow.

CONCLUSIONS

Considering the limitations of Taylor's hypothesis, the QBT proposed by C. Çıray is implemented and validated in the present study. Energy spectrums are obtained by the spectral study, and the wavenumbers and other related results are determined using a standard computer code written by following the mathematical procedure of QBT. The present results are compared with length scales in the boundary layer of Dogan et al [Dogan, Hanson and Ganapathisubramani, 2016]. Also, MVG data from the ongoing PhD research of Akpolat is analyzed by the same method. The results in all frequency ranges of the spectrums of the chosen measurement points are consistent with those of the previous studies in the literature such as -5/3 slope in inertial subrange and quick dissipation in range of the energy dissipating eddies. Also, it is observed that the QBT provides realistic results for large eddies. As a result of these analyses, all information of eddies such as sizes, life spans, and energies can be obtained.

Additionally, the length scales found by QBT are compared with the ones used in Dogan et al.'s study. It is found that the results are significantly different from each other. The scales obtained by QBT are smaller than the used ones in the compared study, specifically, the scales of the largest eddies and the most energetic eddies.

To summarize, these length scales, which form the basis of many studies on turbulent flow problems and frequently used in turbulence models, are calculated for the boundary layer experiments using the QBT. The results obtained by the QBT provide more realistic information about eddies and the characteristics of the flow as comparing with those of Taylor's hypothesis. In the continuation of the study, it is aimed to continue by analyzing other types of the flows by this approach.

ACKNOWLEDGEMENTS

First of all, the authors gratefully acknowledge Dr. E. Doğan for providing her experimental data that was obtained as part of her doctoral studies at the University of Southampton and making this study possible. Also, the authors gratefully acknowledge M.Tuğrul Akpolat for sharing the experimental data obtained for his ongoing PhD reserach. Especially, authors thank Prof. Dr. C. Çelenligil (from Aerospace Eng. Dept. METU) for his contribution to the careful review of the study. Also, the authors appreciate the support of Dr. M. Perçin (from Aerospace Eng. Dept. METU).

References

Akpolat, M., T., Abdulrahim, A., Hassanein, A., Uzol, O. and Perçin, M. (2021) *Experimental Characterization of Micro Vortex Generators in Low Speed Flows*, AIAC

Castro, I. P. (1984) *Effects of free stream turbulence on low Reynolds number boundary layers.* J. Fluids Engng 106, 298–306.

Ciray, C. (1980) *On wave number definition in turbulence*, METU Journal of Pure and Applied Sciences Vol 13, No 3, pp: 431-480.

Ciray, C. (2013) *Akışkanlar Mekaniğine Giriş Üçüncü Kitap*, Odtü Yayıncılık, 2013.

Ciray, C. (2017) *Wave number in turbulence and its discrete nature*, AIAC X 041.

Ciray, C. (2019) *Quantic behaviour of turbulence*, AIAC X 044.

Ciray, C. (2020) *Türbülansın bir problemi ve 'Türbülansın quantik davranışı' yaklaşımıyla çözümü*, UHUK.

de Kat, R. and Ganapathisubramani, B. (2015) *Frequency–wavenumber mapping in turbulent shear flows.*, Journal of Fluid Mechanics, 783, 166-190.

del Alamo, J. C. and Jimenez J. (2009) *Estimation of Turbulent Convection Velocities and Corrections to Taylor's Approximation*, Journal of Fluid Mechanics.

Dogan, E., Hanson, R. and Ganapathisubramani, B. (2016) *Interactions of large scale free stream turbulence with turbulent boundary layers*, Journal of Fluid Mechanics 1-29.

Mydlarski, L. and Warhaft, Z. (1996) *On the onset of high-Reynolds-number grid-generated wind tunnel turbulence*. J. Fluid Mech. 320, 331–368.

Perry, A. E. and Li, J. D. (1990) *Experimental support for the attached-eddy hypothesis in zero pressure gradient turbulent boundary layers*. J. Fluid Mech. 218, 405–438.

Reynolds, O. (1895) *IV. On the dynamical theory of incompressible viscous fluids and the determination of the criterion.*, Philosophical transactions of the royal society of london .(a.), (186), 123 164.

Stull, R. B. (2012) *An introduction to boundary layer meteorology (Vol. 13)*, Springer Science & Business Media , 5 7.

Sun, Z. (2015) *Micro Vortex Generators for Boundary Layer Control: Principles and Applications.*, International Journal of Flow Control, 7(1-2), 67-86

Taylor, G. I. (1938) *The spectrum of turbulence*, Proceedings of the Royal Society of London. Series A Mathematical and Physical Sciences 164 (919), 476 490.

Tennekes, H. and Lumley, J. L. (1972) *A First Course in Turbulence.*, MIT Press, . 65–66.

Townsend, A. A. (1976) *The Structure of Turbulent Shear Flow.*, 2d ed., Cambridge University Press, . 46–47.

Yang, X. I. A. and Howland, M. F. (2018) *Implication of Taylor's hypothesis on measuring flow modulation.*, Journal of Fluid Mechanics, 836, 222.

Zaman, K. B. M. Q. and Hussain, A. K. M. F. (1981) *Taylor hypothesis and large-scale coherent structures.*, Journal of Fluid Mechanics, 112, 379-396.